

Interaction-induced coherence among polar bosons stored in triple-well potentials

Bo Xiong and Uwe R. Fischer

*Seoul National University, Department of Physics and Astronomy
Center for Theoretical Physics, 151-747 Seoul, Korea*

(Dated: December 13, 2012)

We study first-order spatial coherence for interacting polar bosons trapped in triple-well potentials. It is argued that besides the well-known coherence-producing couplings related to tunneling between the sites, there exists coherence based solely on intersite interactions, which prevails between the outer sites of the triple well when their total filling is odd. We find that it originates from the superposition of two degenerate many-body states in symmetric triple wells, and demonstrate its robustness against perturbations due to various tunneling mechanisms and pair exchange.

PACS numbers: 03.75.Lm, 73.43.Nq

I. INTRODUCTION

The study of the many-body physics of interacting particles stored in multiple-well geometries or periodic lattices has wide-ranging implications for the cross-fertilization of condensed-matter physics and quantum optics [1]. Preparing ultracold polar molecules in such external scalar potentials possessing local minima, offers manifold opportunities to investigate the intricate phase diagrams related to the complex coherence properties implied by the long-range dipolar interactions between the molecules. In the simplest version of the Hubbard model with contact interactions only, the existence of first-order coherence is conventionally associated to the competition between kinetic (tunneling) energy and two-body interactions. By contrast, the existence of several energy scales associated with the nonlocal two-body interactions vastly enriches the structure of the phase diagram [2], and enables the creation of many phases with distinct coherence properties.

For the observation of the effects of nonlocal interactions, a triple-well potential is among the conceptually simplest setups to present features which go beyond those of contact interactions. A major advantage of the triple well is that it is tractable numerically, e.g. for the ground state by exact diagonalization (ED), for a comparatively large number of bosons when the field operator expansion is restricted to the lowest-lying orbital per site, so that only three field-operator modes are involved. In optical lattice terminology, this would be referred to as the single-band Bose-Hubbard model [3]. Previous theoretical work has explored bosonic triple-well systems for contact interactions by a semiclassical approach [4], mean-field treatments [5, 6], and the multiconfigurational time-dependent Hartree method for bosons [7]. Transistor-like effects in a triple well, where the occupation of the middle well controls tunneling between the outer wells were demonstrated in [8]. Polar bosons in triple-well potentials, including however only the conventional single-particle tunneling mechanism, have been investigated by many-body [9] and mean-field methods [10].

In what follows, we demonstrate that a triple well storing polar bosons with dipolar interactions can exhibit

variants of the first-order coherence of matter waves of physically distinct origins. Besides the coherence due to single-particle and occupation-number-weighted tunneling we show that, in the appropriate parameter regime, the intersite interaction can generate macroscopic first-order coherence between the two outer sites of the triple well, in the absence of any kind of tunneling. We demonstrate both the origin of this interaction-induced coherence and its stability against perturbations due to various tunneling mechanisms (both conventional short-range and long-range) as well as pair exchange. We also point out that a possible destabilization by a possible asymmetry of the trap potential can be counteracted by a small amount of occupation-number-weighted tunneling, which stems from interactions, and analyze the finite-temperature behavior of the interaction-induced coherence and propose its possible measurement. Finally, we discuss specific features of the phase diagram of the triple well related to pair exchange and occupation-number-weighted tunneling, establishing *inter alia* a procedure to measure the latter.

II. TRIPLE WELL HAMILTONIAN

We consider N dipolar bosons trapped in triple-well potentials where both the potential depth in each well and the relative orientation of the polarized dipoles is adjustable [9, 10]. It is furthermore assumed that the lowest-energy orbital wavefunction in each well, $\phi_i(\mathbf{r})$, where i denotes the well index, is fixed and independent of the particle numbers per site (the filling). The dipole moment of the bosons is sufficiently strong in the sense that a large dipole coupling dominates the contact interaction coupling; this is realistically obtained with ultracold polar molecules with large permanent electric dipole moment [11]. Expressing the bosonic field operator as $\hat{\psi}(\mathbf{r}) = \sum_{i=1}^3 \phi_i(\mathbf{r}) \hat{a}_i$, the low-energy Hamiltonian for the

triple well is of the single-band Bose-Hubbard form

$$\begin{aligned} \hat{H} = & -J_1[\hat{a}_2^\dagger(\hat{a}_1 + \hat{a}_3) + \text{h.c.}] - J_2[\hat{a}_2^\dagger(\hat{n}_2 + \hat{n}_1)\hat{a}_1 + \text{h.c.}] \\ & - J_2[\hat{a}_2^\dagger(\hat{n}_2 + \hat{n}_3)\hat{a}_3 + \text{h.c.}] - \frac{J_2}{\alpha}[\hat{a}_1^\dagger(\hat{n}_1 + \hat{n}_3)\hat{a}_3 + \text{h.c.}] \\ & + \frac{W}{2}[(\hat{a}_2^\dagger)^2(\hat{a}_1^2 + \hat{a}_3^2) + \text{h.c.}] + \frac{W}{2\alpha}[(\hat{a}_1^\dagger)^2\hat{a}_3^2 + \text{h.c.}] \\ & + \frac{U}{2}\sum_{i=1}^3\hat{n}_i(\hat{n}_i - 1) + V\left[\hat{n}_1\hat{n}_2 + \hat{n}_2\hat{n}_3 + \frac{1}{\alpha}\hat{n}_1\hat{n}_3\right] \\ & + \sum_{i=1}^3\epsilon\hat{n}_i + \delta E\hat{n}_1. \end{aligned} \quad (1)$$

Here $J_1 = -\int d\mathbf{r}\phi_i^*(\mathbf{r})[-\nabla^2/2m + V_{\text{trap}}(\mathbf{r})]\phi_{i+1}(\mathbf{r})$ (with V_{trap} the triple well scalar potential and we set $\hbar = 1$), $J_2 = -\int |\phi_i(\mathbf{r})|^2\phi_i^*(\mathbf{r}')\phi_{i+1}(\mathbf{r}')V_{\text{dd}}(\mathbf{r} - \mathbf{r}')d\mathbf{r}d\mathbf{r}'$, and $W = \int \phi_i^*(\mathbf{r})\phi_i^*(\mathbf{r}')\phi_{i+1}(\mathbf{r})\phi_{i+1}(\mathbf{r}')V_{\text{dd}}(\mathbf{r} - \mathbf{r}')d\mathbf{r}d\mathbf{r}'$ are the single-particle, occupation-number-weighted, and pair-tunneling rates respectively [12, 13]. The couplings $U = g\int |\phi_i(\mathbf{r})|^4d\mathbf{r} + \int |\phi_i(\mathbf{r})|^2|\phi_i(\mathbf{r}')|^2V_{\text{dd}}(\mathbf{r} - \mathbf{r}')d\mathbf{r}d\mathbf{r}'$ characterizes the on-site interaction, and $V = \int |\phi_i(\mathbf{r})|^2|\phi_{i+1}(\mathbf{r}')|^2V_{\text{dd}}(\mathbf{r} - \mathbf{r}')d\mathbf{r}d\mathbf{r}'$ is due to dipolar-interaction-induced coupling between sites; we neglect the contribution of the contact contribution to the J_2, V, W terms. Finally, ϵ represents identical single-particle energies at each site and δE denotes a bias energy applied to site 1, while $g = 4\pi a_s/m$ is the short-range interaction constant with a_s the s -wave scattering length. The term $\sum_{i=1}^3\epsilon\hat{n}_i = \epsilon\hat{N}$ is displayed for completeness here, even though it adds only a constant to the Hamiltonian: We choose ϵ as the (arbitrary) energy scale below.

The dipolar interaction between polarized dipoles at positions \mathbf{r}, \mathbf{r}' is given by $V_{\text{dd}}(\mathbf{r} - \mathbf{r}') = d^2(1 - 3\cos^2\theta)/|\mathbf{r} - \mathbf{r}'|^3$, where θ is the angle between $\mathbf{r} - \mathbf{r}'$ and the dipole moment \mathbf{d} . $d^2 = \mu_0\mu^2/(4\pi)$ and $\bar{d}^2/(4\pi\epsilon_0)$ for magnetic and electric dipoles, respectively, where μ is the magnetic dipole moment and \bar{d} is the electric dipole moment. From point-like, tightly localized orbitals $\phi_i(\mathbf{r})$ to two infinite chains of dipoles where the width of two aligned orbitals is much larger than its separation (e.g., in Fig. 6 below, the condition $\sigma_y \gg \sigma_z$ amounts to two infinite chains of dipoles), the factor α for intersite interactions varies from 8 to 4 [9]. The ratios α of next-nearest-neighbor and nearest-neighbor sites vary in general somewhat for the contributions J_2, W , and V , respectively, depending on the geometry of the triple-well potentials and the overlap of orbital wavefunctions. For simplicity and because it does not affect our main conclusions below, we take their ratio factors α to be equal; we choose $\alpha = 8$.

We include the pair tunneling W , which has been shown to decide on the question of coherent versus fragmented many-body states in general two-mode models [14]. On an optical lattice, it was subsequently demonstrated that pair-tunneling can change significantly the phase diagram of polar bosons in the extended Bose-Hubbard model [13].

The fundamental object of interest in what follows, the many-body wavefunction, can generally be expanded in

a Fock basis,

$$|\Psi\rangle = \sum_{n_1, n_2, n_3} f(n_1, n_2, n_3)|n_1, n_2, n_3\rangle, \quad (2)$$

where $n_1 + n_2 + n_3 = N$.

III. VARIANTS OF COHERENCE

A. Vanishing tunneling couplings

In the absence of any tunneling, i.e., $J_1 = J_2 = W = 0$, the total energy of the triple-well system subject to the Hamiltonian (1) reads,

$$E(n_1, n_3) = (V - U)(N - n_1 - n_3)[n_1 + n_3] + (V/\alpha - U)n_1n_3. \quad (3)$$

We concisely review the phase diagram of polar bosons in a triple well as found in [9]. Phase A, cf. Fig. 1, is characterized by $n_1 = n_3, n_2 \neq 0$, and appears for $U > 0$ and $V \leq \frac{8}{15}U$, and $U < 0$ and $V < 8U$. Phase B occurs for $n_1 = n_3 = \frac{N}{2}, n_2 = 0$, for $\frac{8}{15}U < V \leq 8U$ and $U > 0$. The case that $V \geq U$ for $U < 0$, as well as $V > 8U$ for $U > 0$ leads to the phase C where $n_1 = n_3 = 0$. Finally, for phase D macroscopic states with $n_1 = 0$ and $n_3 \neq 0$ and $n_1 \neq 0$ and $n_3 = 0$ are coherently superposed in a Schrödinger cat type state, where the regime of parameters is $U < 0$ and $8U < V < U$.

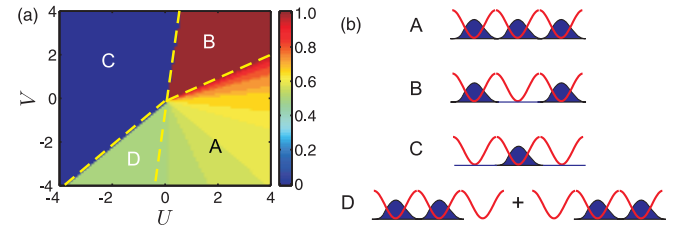


FIG. 1. (color online) (a) Phase diagram in terms of the magnitude of $n/N \equiv \langle \hat{n}_1 + \hat{n}_3 \rangle / N$ as a function of U and V for $N = 30, J_1 = J_2 = W = 0$. The dashed lines in panel (a) show the boundaries between the phases A–D that are shown schematically in (b).

We now point out that in Ref. [9], an important property of phase A has been overlooked. For phase A, in which n_2 is restricted to be integer by the fact that this minimizes the energy Eq. (3), both n_1 and n_3 can be fractional (and not only integer, as stated in [9]). We found, as also numerically verified by ED, that when the average fillings in each site, $\bar{n}_i \equiv \langle \hat{n}_i \rangle$ fulfill $n \equiv \bar{n}_1 + \bar{n}_3$ is odd, so that \bar{n}_1 and \bar{n}_3 are *fractional* there exist two-fold degenerate states in phase A, with the degenerate subspace spanned by the two states

$$\begin{aligned} |\Psi_1\rangle &= |(n-1)/2, N-n, (n+1)/2\rangle, \\ |\Psi_2\rangle &= |(n+1)/2, N-n, (n-1)/2\rangle. \end{aligned} \quad (4)$$

On the other hand, when n is even, the many-body state is a single Fock state, $|\Psi\rangle = |n/2, N-n, n/2\rangle$. All off-diagonal first-order coherence matrix elements are then zero, i.e., $g_{12}^{(1)} = g_{23}^{(1)} = g_{13}^{(1)} = 0$. This is, however, not the case for a superposition of the states in Eq. (4), as we will now argue.

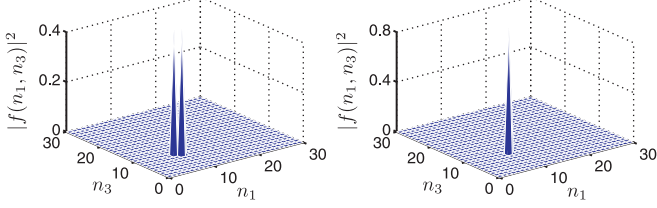


FIG. 2. (color online) Distribution of many-body amplitudes in the wave function (2) for $N = 30$ particles and odd $n = 17$ (left, $U = 2.5, V = -3, N = 30, n = 17$) and even $n = 18$ (right, $U = 4, V = -3$). The switching between the double- and single-peak structures corresponds to the “coherence fan” structure in shown 3, where macroscopic coherence between sites 1 and 3 is obtained only for odd n . The double-peak structure on the left is robustly obtained also when small tunneling couplings are turned on, cf. Fig. 3 (b)–(d).

The many-body state is in general any linear combination of two degenerate states, i.e., $|\Psi\rangle = \alpha|\Psi_1\rangle + \beta|\Psi_2\rangle$ where the coefficients α and β can be any complex number and fulfill $|\alpha|^2 + |\beta|^2 = 1$. However, for any small tunneling in a realistic system, e.g., any small J_1, J_2 , or W , α and β adjust to relative phase zero. Moreover, the spatial symmetry between sites 1 and 3 requires $\bar{n}_1 = \bar{n}_3$. The only possible form of the many-body wavefunction then is $|\Psi\rangle = \frac{e^{i\theta}}{\sqrt{2}}[|\Psi_1\rangle + |\Psi_2\rangle]$, with some global phase θ . Setting the latter to zero, we conclude that

$$|\Psi\rangle = \frac{1}{\sqrt{2}}[|\Psi_1\rangle + |\Psi_2\rangle]. \quad (5)$$

The above many-body state induces macroscopically large nonlocal first-order coherence, i.e., the quantity

$$g_{13}^{(1)} = \frac{1}{2\bar{n}} \left[\langle \Psi | \hat{a}_1^\dagger \hat{a}_3 | \Psi \rangle + \text{h.c.} \right] = \frac{n+1}{4\bar{n}} \quad (6)$$

is of order unity, cf. Fig. 3, where $\bar{n} = \sum_{i=1}^3 \bar{n}_i/3$.

We stress that the interaction-induced coherence only exists between the outer sites of the triple well, i.e., $g_{12}^{(1)} = g_{23}^{(1)} = 0$ and $g_{13}^{(1)} = \frac{n+1}{4\bar{n}}$. The single-particle density matrix indeed has three macroscopic eigenvalues, which are $\frac{3n+1}{4}$, $\frac{n-1}{4}$, and $N-n$. This demonstrates that, seen from the point of view of the *entire* triple well, the superposed states with macroscopic interaction-induced coherence between the outer sites, are globally speaking fragmented condensate states [15].

We point out that the superposition (5) of two-fold degenerate states is much more robust than the degenerate states occurring in phase C. For vanishing tunneling, the many-body wavefunction in the parameter regime of phase C should be any of three degenerate states, i.e.,

$|\Psi\rangle = a|N, 0, 0\rangle + b|0, N, 0\rangle + c|0, 0, N\rangle$ where any two of a, b , and c are zero and the remaining one unity. But this tri-fold degeneracy is broken readily against a small perturbation of first-order coupling, e.g., the single-particle tunneling between wells, and the many-body wavefunction favors the single-particle state $|0, N, 0\rangle$. By contrast, a small perturbation due to tunneling does not destroy the degeneracy of $|\Psi_1\rangle$ and $|\Psi_2\rangle$, as we will demonstrate in the following subsection.

B. Finite tunneling couplings

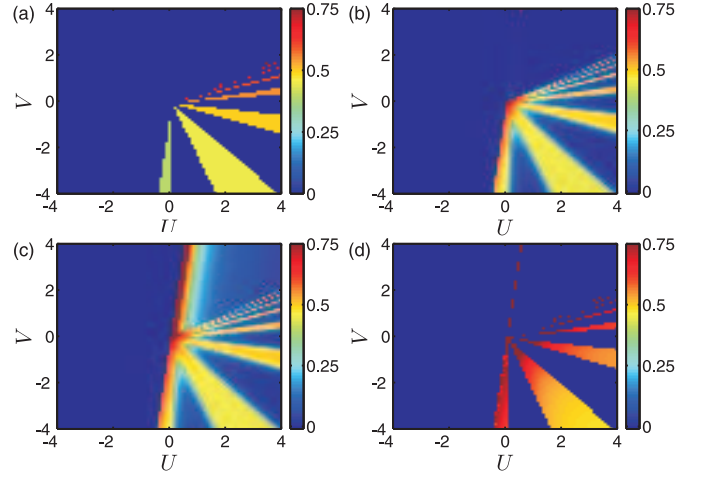


FIG. 3. (color online) Illustration of the insensitivity of the “fan” structure of the coherence function $g_{13}^{(1)}$, related to the phase transitions between even and odd values of n for varying tunneling couplings. Magnitude of $g_{13}^{(1)}$ for (a) no tunneling, $J_1 = J_2 = W = 0$, (b) $J_1 = 0.02$, and $J_2 = W = 0$, (c) $J_2 = 0.001$, and $J_1 = W = 0$, (d) $W = -0.02$, and $J_1 = J_2 = 0$; $N = 30$ in all plots.

The emergence of the first-order coherence for $n = \text{odd}$ and disappearance for $n = \text{even}$ results in the formation of a fan structure of the first-order coherence in the parameter regime of phase A, see Fig. 3. To explain the structure of the phase diagram in region A of the phase diagram in more detail, we now argue that while a small amount of single-particle, occupation-number-weighted, or pair tunneling slightly broadens the statistical distribution of the many-body wavefunction (2) around the superposed state in Fock space, it does not change the structure of the phase diagram. For concreteness, with a finite but small J_1 , the many-body wavefunction should be of the form,

$$\begin{aligned} |\Psi\rangle = & c_1|(n-1)/2, N-n, (n+1)/2\rangle \\ & + c_2|(n+1)/2, N-n, (n-1)/2\rangle \\ & + c_3|(n-3)/2, N-n, (n+3)/2\rangle \\ & + c_4|(n+3)/2, N-n, (n-3)/2\rangle \\ & + \text{other terms} \dots, \end{aligned} \quad (7)$$

where the additional single-particle states are determined by J_1 and the larger J_1 , the more single-particle states need to be included. For small J_1 , c_1 and c_2 are dominant, and determined by U and V , such that the interaction-induced coherence is obtained. Only with strongly increasing J_1 , the contributions of more single-particle states broaden the distribution of the many-body state in Fock space, significantly reducing the value of c_1 and c_2 , and then suppressing the interaction-induced coherence. A similar discussion can be applied to the couplings J_2 and W . Therefore, effects caused by the various tunnelings do not result in an essential change for the interaction-induced coherence, as long as the tunneling perturbations remain sufficiently small. This robustness of the coherence against perturbations has been numerically verified by the ED calculations shown in Fig. 3. It can be concluded from Fig. 3 that the magnitude of the coherence changes due to finite tunnelings of various origin. However, the phase boundaries (the “fan” structure), while slightly blurred by small tunneling, remain basically intact. Note for the proper interpretation of the parameter values chosen that the relevant quantities to compare with each other are J_1 and nJ_2 .

By comparing Figs. 3 (b) and (c) we see that the nature of the crossover between the phases B and C is strongly influenced by number-weighted tunneling, while ordinary tunneling has basically no effect on the transition. This highlights the long-range nature of the tunneling mechanism correlated to site occupation, embodied in the J_2 terms. In addition, it furnishes a possible method to *measure* J_2 independently from J_1 in the triple well by investigating the transition region between phases B and C.

We finally conclude from Fig. 3 (d) that the effect of pair-exchanges $\propto W$ on the *single-particle* coherence magnitude is most pronounced, confirming the profound effect pair exchanges have on the first-order coherence [14].

C. Small bias energies

When a small bias energy δE (chosen here to be negative) is accounted for, the actual triple-well ground state should be $|\frac{n+1}{2}, N-n, \frac{n-1}{2}\rangle$ and the associated energy is $(V-U)(N-n)n + (\frac{V}{\alpha} - U)\frac{n^2-1}{4} + \delta E(n + \frac{1}{2})$ while the energy of the superposition state with respect to the Hamiltonian (1) is $(V-U)(N-n)n + (\frac{V}{\alpha} - U)\frac{n^2-1}{4} + \delta E n$ (the superposition (5) is not the eigenstate of the Hamiltonian (1)). Therefore the superposition energy is higher than the ground-state energy by $|\delta E|/2$, indicating that for any asymmetry between sites 1 and 3, the two-fold degeneracy and therefore the coherence is broken. However, for a negative intersite interaction, i.e., $V < 0$, choosing Gaussian orbitals (also see section IV below) shows that J_2 is positive. This implies that J_2 prefers the superposed states and stabilizes the interaction-induced coherence states. For a *small* $\delta E < 0$ and $J_2 > 0$, the ansatz for the many-body state can be written $\eta|\frac{n+1}{2}, N-n, \frac{n-1}{2}\rangle + \gamma|\frac{n-1}{2}, N-n, \frac{n+1}{2}\rangle$, where η and γ are real and have equal sign, with normalization $\eta^2 + \gamma^2 = 1$. The energy contributed by the bias δE is $[\frac{n}{2} + \frac{1}{2}(\eta^2 - \gamma^2)]\delta E$, while that of J_2 is $-\frac{J_2}{\alpha}\eta\gamma n(n+1)$. It is then straightforward to obtain that the condition for stabilizing the interaction-induced coherence state is given by $J_2 > \frac{\alpha|\delta E|}{n+1}$ for not too large $|\delta E|$ (for increasing J_2 , more single-particle states need to be included). This condition has been numerically confirmed as well.

D. Detection of interaction-induced coherence

We propose to verify the existence of purely interaction-based coherence with the nonequilibrium dynamics of the nonlocal coherent state. The initially assumed superposition state including the ground-state coherence is quenched towards a nonequilibrium state by breaking suddenly the symmetry of sites 1 and 3, by applying a single-energy site bias to site 1 instantaneously, cf. the illustration in Fig. 4. The time-dependent many-body wavefunction is then of the form,

$$|\Psi(t)\rangle = \frac{1}{\sqrt{2}} \exp \left[-it \left((V-U)(Nn - n^2) + \left(\frac{V}{\alpha} - U \right) \frac{n^2-1}{2} + N\epsilon \right) \right] \sum_{\gamma=\pm} \exp \left[-it\delta E \frac{n+\gamma}{2} \right] \left| \frac{n+\gamma}{2}, N-n, \frac{n-\gamma}{2} \right\rangle \quad (8)$$

where n is assumed to be odd. Therefore, it is obtained readily that

$$\begin{aligned} g_{13}^{(1)} &= \frac{1}{2\bar{n}} \langle \Psi(t) | (\hat{a}_1^\dagger \hat{a}_3 + \text{h.c.}) | \Psi(t) \rangle \\ &= \frac{(n+1)}{4\bar{n}} \cos[\delta E t] \end{aligned} \quad (9)$$

$$g_{12}^{(1)} = g_{23}^{(1)} = 0. \quad (10)$$

Formulas (9) and (10) show that there exists exclusively the time-dependent phase coherence between sites 1 and 3, for which the out-of-equilibrium oscillation frequency is determined by δE , in complete agreement with our numerical results displayed in Fig. 4. The interaction-induced coherence therefore can be measured by means of atomic interference, where at different instants of evolution with respect to the same initial setup, the trap po-

tentials is released such that the freely expanding clouds from sites 1 and 3 will interfere. The visibility of the interference pattern then amounts to a measure of the first-order coherence [16].

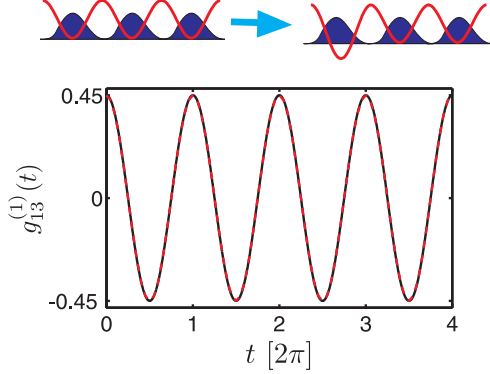


FIG. 4. (color online) Time evolution of $g_{13}^{(1)}(t)$ in the absence of tunneling, $J_1 = J_2 = W = 0$, for an initial state with $U = 1.5$, $V = -2$, and $\delta E = 0$, quenched into $\delta E = -1$ (see schematic representation on top). The black solid line is from a numerical calculation, and the red dashed line from formula (9).

E. Coherence versus temperature

Here, we explore the effect of temperature on the interaction-induced coherence. In the canonical ensemble, the thermal average of an operator \hat{O} is $\langle \hat{O} \rangle = \sum_{j=0}^N \frac{e^{-E_j/T}}{Z} \langle E_j | \hat{O} | E_j \rangle$, where the canonical partition sum $Z = \sum_{j=0}^N e^{-E_j/T}$. In the zero temperature limit, $\langle \hat{O} \rangle$ yields the expectation value of \hat{O} in the ground state. Fig. 5 shows that in the regime of small temperatures, e.g., $T \lesssim 0.5$, $g_{13}^{(1)}(T)$ is only slightly reduced, indicating that the low-energy excitation states do leave the superposed states basically intact. With increasing $T \gtrsim 0.5$, the high-level excitation states yield to a significant reduction of $g_{13}^{(1)}(T)$.

IV. EXPERIMENTAL SETUP AND PARAMETER CORRELATIONS

We now discuss experimental feasibility and realistic parameter values for dipolar interactions. Ref. [9] provided a rather detailed scheme of how to realize the required triple well configuration experimentally. In particular, using an acousto-optic modulator to toggle the dimple formed by optical potentials between several positions at high rate to create almost arbitrary time-averaged potentials [17] can be applied to our case to adjust the single-energy offsets. It should not be difficult for existing experiments to reach the parameter regime of phase A which is quite broad in terms of the values of U and V .

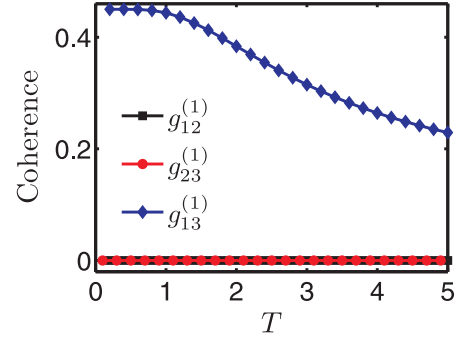


FIG. 5. (color online) The first-order spatial coherence, $g_{ij}^{(1)}(T)$ as a function of temperature, with $U = 2.5$, $V = -3$, $N = 30$, and $J_1 = J_2 = W = 0$.

We suggest to realize the interaction-induced coherence in small samples because large atom numbers suppresses the fan structure window size shown in Fig. 3.

A triple-pancake trap 2D configuration to achieve $U > 0$ and $V < 0$ is shown in Fig. 6. To understand the parameter relation between V , J_2 , and W , we take as the low-energy approximations to the exact Wannier states orbital wavefunctions corresponding to the harmonic-oscillator ground-states at each well [18]. Specifically the single-particle orbitals are assumed to be of the form,

$$\begin{aligned} \phi_1(\mathbf{r}) &= \frac{1}{\sqrt{2\pi\sigma_z\sigma_y}} \exp \left[-\frac{z^2}{4\sigma_z^2} - \frac{y^2}{4\sigma_y^2} \right] \delta(x), \\ \phi_2(\mathbf{r}) &= \frac{1}{\sqrt{2\pi\sigma_z\sigma_y}} \exp \left[-\frac{(z-l)^2}{4\sigma_z^2} - \frac{y^2}{4\sigma_y^2} \right] \delta(x), \\ \phi_3(\mathbf{r}) &= \frac{1}{\sqrt{2\pi\sigma_z\sigma_y}} \exp \left[-\frac{(z-2l)^2}{4\sigma_z^2} - \frac{y^2}{4\sigma_y^2} \right] \delta(x). \end{aligned} \quad (11)$$

We take the separation of the two nearest-neighbor orbital wavefunctions, l , as the unit of length and σ_z to obtain the relation of $-J_2/V$ and W/V as shown in Fig. 7 (the ratios are independent of σ_y). The numerical results upon evaluating the parameter ratios show that $J_2 > 0$ and $W < 0$ are consistently smaller than $|V|$, and with

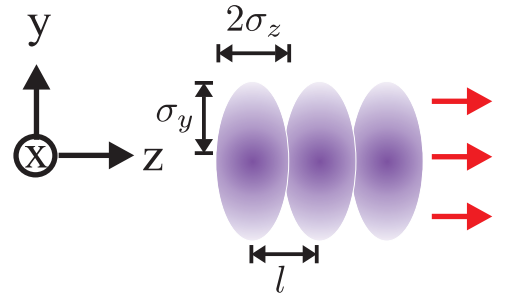


FIG. 6. (color online) The configuration of a triple pancake system where the three 2D pancakes are aligned along the \hat{y} direction, and all dipoles are oriented along \hat{z} (red arrows), such that $U > 0$ and $V < 0$.

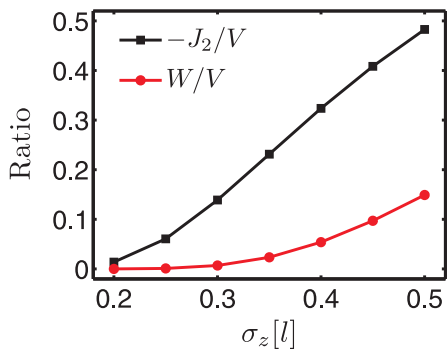


FIG. 7. (color online) The ratios $-J_2/V$ and W/V for various values of the Gaussian width σ_z , cf. Fig. 6. Filled squares ($-J_2/V$) and circles (W/V) are numerically evaluated data points, and lines are a guide to the eye.

increasing overlap of two orbital wavefunctions, the ratios $-J_2/V$ and W/V increase monotonically (see Fig. 7). By contrast, for contact interaction, W/V is constant and $-J_2/V \gg 1$ for small overlap, *decreasing* with increasing overlap [18]. This indicates that the dipole-dipole interaction tends to enhance the interaction-induced number-weighted tunneling over the nearest-neighbor interaction coupling for increasing overlap (in the setup of Fig. 7), while contact interactions have the opposite effect.

V. CONCLUSION

We have shown that intersite interaction in a triple well, due to large dipole-dipole interactions, in a broad parameter regime, can generate macroscopic first-order coherence between the two outer sites, in the absence of tunneling between any of the three sites. This interaction-induced coherence originates from the superposition of two degenerate states of polar bosons in a symmetric triple-well potential. While globally the many-body state is fragmented, it exhibits this partial coherence between the modes localized on the outer

sites, which is robust against tunneling perturbations and against pair exchanges. We have also demonstrated that the fragility of the coherence against site biases (a mismatch of energy minima lifting the degeneracy) can be counterbalanced by a small contribution of occupation-number-weighted tunneling.

The interaction-induced coherence between sites 1 and 3 executes Josephson oscillations when the initial superposition state is quenched towards a nonequilibrium state by suddenly breaking the symmetry of the triple well (rapidly turning on a site bias), where the associated oscillation frequency is determined by the bias. This provides an experimental method to measure the strength of the interaction-induced mesoscopic coherence between the outer sites of the triple well.

Finally, we note that there exists a recent work in which it was shown that repulsive interactions induce first-order correlation between spatially separated chains of one-dimensional dipolar fermions [19]. Our origin of coherence is determined by both the spatial symmetry of the triple well and the intersite interaction. On the other hand, due to the existence of many degenerate states in a very narrow window of intertube interactions in the fermionic system, an infinitely small intertube tunneling can mix many degenerate states, and then lead to a coherent ground state. Although the nonlocal interaction coupling V is the crucial factor in both cases, the interaction in the fermionic case is repulsive, i.e., $V > 0$, in distinction to the present case of elementary bosons, where the first-order coherence arises from negative V . In addition, the coherent-state regime for V is very narrow in the fermionic system, in contrast to the bosonic triple well, where V and U cover a wide area in parameter space.

ACKNOWLEDGMENTS

This research was supported by the NRF Korea, grant Nos. 2010-0013103 and 2011-0029541, and the Seoul National University Foundation Research Expense.

-
- [1] M. Lewenstein, A. Sanpera, V. Ahufinger, B. Damski, A. Sen(De), U. Sen, *Adv. Phys.* **56**, 243 (2007).
 - [2] C. Trefzger, C. Menotti, B. Capogrosso-Sansone, and M. Lewenstein, *J. Phys. B: At. Mol. Opt. Phys.* **44**, 193001 (2011).
 - [3] D. Jaksch and P. Zoller, *Annals of Physics* **315**, 52 (2005).
 - [4] S. Mossmann and C. Jung, *Phys. Rev. A* **74**, 033601 (2006).
 - [5] E. M. Graefe, H. J. Korsch, and D. Witthaut, *Phys. Rev. A* **73**, 013617 (2006).
 - [6] P. Buonsante, R. Franzosi, and V. Penna, *Phys. Rev. Lett.* **90**, 050404 (2003).
 - [7] A. I. Streltsov, K. Sakmann, O. E. Alon, and L. S. Cederbaum, *Phys. Rev. A* **83**, 043604 (2011).
 - [8] J. A. Stickney, D. Z. Anderson, and A. A. Zozulya, *Phys. Rev. A* **75**, 013608 (2007).
 - [9] T. Lahaye, T. Pfau, and L. Santos, *Phys. Rev. Lett.* **104**, 170404 (2010).
 - [10] D. Peter, K. Pawłowski, T. Pfau, and K. Rzążewski, *J. Phys. B* **45**, 225302 (2012).
 - [11] M. A. Baranov, *Phys. Rep.* **464**, 71 (2008).
 - [12] A. Bühler and H. P. Büchler, *Phys. Rev. A* **84**, 023607 (2011).
 - [13] T. Sowiński, O. Dutta, P. Hauke, L. Tagliacozzo, and M. Lewenstein, *Phys. Rev. Lett.* **108**, 115301 (2012).

- [14] P. Bader and U. R. Fischer, Phys. Rev. Lett. **103**, 060402 (2009).
- [15] O. Penrose and L. Onsager, Phys. Rev. **104**, 576 (1956).
- [16] F. Gerbier *et al.*, Phys. Rev. Lett. **101**, 155303 (2008).
- [17] K. Henderson, C. Ryu, C. MacCormick and M. G. Boshier, New J. Phys. **11**, 043030 (2009).
- [18] G. Mazzaella, S. M. Giampaolo, and F. Illuminati, Phys. Rev. A **73**, 013625 (2006).
- [19] C.-M. Chang, W.-C. Shen, C.-Y. Lai, P. Chen, and D.-W. Wang, Phys. Rev. A **79**, 053630 (2009).